chemistry

Article

Exploiting Supramolecular Synthons in Cocrystals of Two Racetams with 4-Hydroxybenzoic Acid and 4-Hydroxybenzamide Coformers

Jason Marquez [1], Egor Novikov [1], Sergei Rigin [1,2], Marina S. Fonari [1,3], Raúl Castañeda [1], Tatiana Kornilova [1] and Tatiana V. Timofeeva [1,*]

[1] Department of Chemistry, New Mexico Highlands University, Las Vegas, NM 87701, USA; jmarquez10@live.nmhu.edu (J.M.); enovikov@live.nmhu.edu (E.N.); rigindale@gmail.com (S.R.); fonari.xray@gmail.com (M.S.F.); lrcastaneda@nmhu.edu (R.C.); tkornilova@live.nmhu.edu (T.K.)
[2] Department of Materials Science and Engineering, North Carolina State University, Raleigh, NC 27606, USA
[3] Institute of Applied Physics, Moldova State University, Academiei Str. 5, MD2028 Chisinau, Moldova
[*] Correspondence: tvtimofeeva@nmhu.edu

Abstract: Structures of three cocrystals of nootropic racetams were studied. They included two cocrystals of phenylpiracetam (**PPA**) with 4-hydroxybenzoic acid (**HBA**) with different stoichiometries, **PPA·HBA** and **PPA·2HBA**, and cocrystal of 2-(4-phenyl-2-oxopyrrolidin-1-yl)-N′-isopropylideneacetohydrazide (**PPAH**) with 4-hydroxybenzamide (**HBD**), **PPAH·HBD**·(acetone solvate). X-ray study of the pure forms of **PPA** and **PPAH** was also carried out to identify variations of molecular synthons under the influence of conformers. The cocrystal structures revealed the diversity of supramolecular synthons namely, amide-amide, amide-acid, acid-acid, and hydroxyl-hydroxyl; however, very similar molecular chains were found in **PPA** and **PPA·2HBA**, and similar molecular dimers in **PPAH** and **PPAH·HBD**. In addition, conformational molecular diversity was observed as disorder in **PPA·2HBA** as it was observed earlier for *rac*-**PPA** that allows for the consideration that cocrystal as an example of partial solid solution. Quantum chemical calculations of **PPA** and **PPAH** conformers demonstrated that for most conformers, energy differences do not exceed 2 kcal/mol that suggests the influence of packing conditions (in this case *R*- and *S*-enantiomers intend to occupy the same molecular position in crystal) on molecular conformation.

Keywords: racetams; phenylpiracetam; X-ray; supramolecular synthon; hydrogen bond; conformation

Citation: Marquez, J.; Novikov, E.; Rigin, S.; Fonari, M.S.; Castañeda, R.; Kornilova, T.; Timofeeva, T.V. Exploiting Supramolecular Synthons in Cocrystals of Two Racetams with 4-Hydroxybenzoic Acid and 4-Hydroxybenzamide Coformers. *Chemistry* **2023**, *5*, 1089–1100. https://doi.org/10.3390/chemistry5020074

Academic Editor: Katharina M. Fromm

Received: 18 April 2023
Revised: 3 May 2023
Accepted: 4 May 2023
Published: 8 May 2023

1. Introduction

Currently there is a significant interest in pharmaceutical materials that can be used for treatment of central nervous system (CNS) disorders. One of the groups of such materials is nootropics that are prescribed as drugs or supplements to improve memory, focus, and cognitive performance. Racetams (piracetam and its derivatives) are nootropic agents known since the 1970s [1–4]. Depending on their substituents, they have different degrees of pharmacological activity.

Nootropil (2-oxo-1-pyrrolidinyl-acetamide, piracetam, **PA**, Scheme 1) was marketed by the United Collection Bureau (UCB) to treat memory and balance problems [5]. The physiological action and structural peculiarities of **PA** have been studied thoroughly. This compound of one hydrate and five anhydrous crystalline forms was documented by Fabbiani et al. [6].

In search for nootropics with improved physicochemical properties, significant efforts were addressed to the **PA** cocrystals [7–11]. Zaworotko at al. [11] demonstrated the importance of supramolecular homo- and heterosynthons in crystal engineering of active pharmaceutical ingredients (APIs) for an explanation and prediction of polymorphic and cocrystalline forms of APIs. This paradigm looks significantly important for nonionized drugs like racetams since it depicts the relative ease with which pharmaceutical cocrystals can be prepared and diversified from the view point of their composition and physical properties. Several examples revealed the successful exploiting of carboxylic acid—primary amide supramolecular heterosynthon in crystal engineering of cocrystals including those that contain two APIs [12–15]. Among published examples of **PA** cocrystals containing two APIs, to mention a few, are carbamazepine with **PA** [8], 2,6-diaminopyridine with **PA** [9], myricetin with **PA** [16]. Viertelhaus et al. obtained six **PA** cocrystals with different organic acids [10]. Cocrystal screening through structural resemblance for eleven **PA** cocrystals with ten different acids was reported by Leyssens et al. [17]. Those examples demonstrated that the amide-carboxylic acid heterosynthon was rarely found in the crystal structures in the presence of additional hydrogen bond donors and acceptors. An example of significant change of properties by cocrystallization is **PA**—*L*-tartaric acid cocrystal. It was found that a reversible water adsorption with a maximum water uptake of 3% was observed for this cocrystal, while for pure **PA** it was more than 40% [10]. Such a drop of hygroscopicity is important for the pharmaceutical industry. An interesting peculiarity of **PA**-hydroquinone cocrystal [8] was that both coformers produced separate parallel 1D motifs of H-bonded **PA** and hydroquinone molecules. In paper [18] multi-component crystallization conditions of several APIs including **PA** allowed for obtaining new polymorph modifications and solvates of APIs.

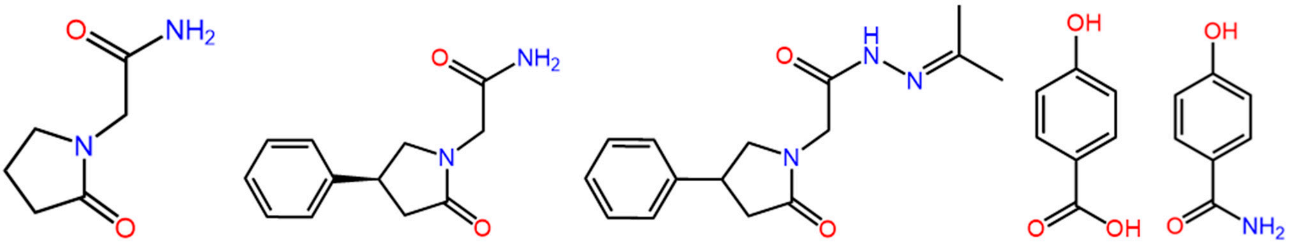

PA PPA, *S*-stereoisomer PPAH HBA HBD

Scheme 1. Structural formulas of piracetam (**PA**), *S*-phenylpiracetam (*S*-**PPA**), 2-(4-phenyl-2-oxopyrrolidin-1-yl)-N′-isopropylideneacetohydrazide (**PPAH**), and coformers 4-hydroxybenzoic acid (**HBA**) and 4-hydroxybenzamide (**HBD**).

Another member of racetams family, 2-(2-oxo-4-phenyl-1-pyrrolidinyl)acetamide (phenotropil, carphedon, phenylpiracetam, **PPA**, Scheme 1) demonstrates, apart from nootropic properties, strong antidepressant and anxiolytic activity [19]. The molecule of **PPA** contains one chiral center in the pyrrolidine ring. So, **PPA** exists in racemic and two enantiomeric, *R*- and *S*-forms (Scheme 1) [19,20]. Crystallographic data (CSD version 5.43, last update November 2022) are available for *rac*-PPA and polymorphs of *R*- and *S*-enantiomers [20,21]. *Rac*-**PPA** (refcodes QELNEB01, QELNEB) crystallizes in the triclinic *P*-1 space group. Stereoisomers crystallize as orthorhombic (refcode SAMZOY, $P2_12_12_1$ space group) and triclinic (refcode SANBAN, *P*1 space group) polymorphs [19,20]. It should be mentioned that pharmacological activities of *rac*-**PPA** and its *R*- and *S*-enantiomers are different, and the memory-improving activity is only characteristic of *R*-enantiomer [22].

To mask their bitter taste, some racetams including **PA** and **PPA** were cocrystallized with saccharine and zinc saccharinate [7]. Particularly for **PPA**, these attempts resulted in preparation of two crystalline complexes, $ZnSac_2Car$ (Car = carphedon in [7], refcode NEFLOB) as a 1D coordination chain where both carbonyl oxygens of pyrrolidone and amide groups coordinate to two different zinc atoms, and $[ZnSac_2(H_2O)_2]\cdot Car\cdot EtOH\cdot H_2O$ (refcode NEFMOE) as a discrete inclusion compound with carphedon interacting with the $[ZnSac_2(H_2O)_2]$ complex through hydrogen bonding [7]. Apart from the **PPA** pure forms, these are the only two known examples of structurally studied multicomponent **PPA** crystals.

For 2-(4-phenyl-2-oxopyrrolidin-1-yl)-N′-isopropylideneacetohydrazide (**PPAH**, Scheme 1), a relatively new member of racetams family [19], to the best of our knowledge, no crystallographic information is available either for pure **PPAH**, or for its cocrystals.

The goal of this study was a search for new forms of nootropics **PPA** and **PPAH**, and a comparison of molecular synthons found in pure materials, different cocrystalline, and polymorphic forms. As coformers for **PPA** and **PPAH**, we used compounds with molecular structures similar to those which were successfully used for formation of **PA** cocrystals [10,11], such as 4-hydroxybenzoic acid (**HBA**) and 4-hydroxybenzamide (**HBD**). The **HBA** in particular has performed well in cocrystal design with APIs [11,23–26]. Structural, and computational studies were carried out for the following pure and cocrystalline materials: **PPA**, **PPA·HBA**, **PPA·2HBA**, **PPAH**, and **PPAH·HBD**·(acetone solvate).

2. Materials and Methods

2.1. Chemicals and Solvents

Phenylpiracetam powder (100%) was purchased from Purenootropics (Purenootropics.net), and Phenylpiracetam as a supplement in capsules was purchased from BrainMedics. 4-Hydroxybenzoic acid, 4-hydroxybenzamide, and acetone solvent were purchased from Sigma Aldrich and used without purification.

2.2. Synthesis

2.2.1. Synthesis of **PPA·HBA** (1:1) Cocrystal

An amount of 22.0 mg (0.1 mmol) of **PPA** and 14.0 mg (0.1 mmol) of **HBA** were dissolved in 5 mL of acetone at room temperature in a test tube covered with parafilm with a hole. After a week, the solvent had evaporated and crystals were observed.

2.2.2. Synthesis of **PPA·2HBA** (1:2) Cocrystal

An amount of 44.0 mg (0.2 mmol) of **PPA** and 42.0 mg (0.3 mmol) of **HBA** were dissolved in 5 mL of acetone at room temperature in a test tube covered with parafilm with a hole. After a week the solvent had evaporated and crystals were observed.

2.2.3. Synthesis of **PPAH·HBD** Cocrystal

Phenylpiracetam produced by BrainMedics was removed from capsules and used for cocrystallization. After cocrystal was obtained and characterized with single crystal X-ray diffraction analysis, we realized that instead of **PPA** we had its derivative, 2-(4-phenyl-2-oxopyrrolidin-1-yl)-N′-isopropylideneacetohydrazide (**PPAH**) presented in Scheme 1. To be sure that powder from capsules was indeed **PPAH**, we recrystallized it from acetone and the single crystal X-ray study unambiguously confirmed that the substance was **PPAH** not **PPA**. In addition, HPLC analysis was performed to check the purity of the substance from capsules. It demonstrated only one peak that stated the compound from capsules did not have any contaminations.

2.2.4. Synthesis of **PPAH·HBD** Cocrystal

To obtain the cocrystal, **PPAH** (27.0 mg, 0.1 mmol) and **HBD** (14.0 mg, 0.1 mmol) in 1:1 molar ratio were separately dissolved in 5 mL of acetone, filtered, and mixed. The resulting solution was covered with parafilm with small holes for slower evaporation and left at room temperature. Small colorless needles showed up on the vial walls after 24 h. Melting points for **PPAH** (144 °C), **HBD** (161 °C) and 1:1 cocrystal **PPAH·HBD**(acetone solvate) (108 °C) were measured on SRS MeltTemp apparatus. All samples were heated with a heat rate 1 °C/min until the substance was completely liquid.

2.3. Single-Crystal X-ray Diffraction Analysis

X-ray diffraction data for **PPA**, **PPAH**, and **PPA·2HBA** cocrystal, were collected on a SMART APEX II CCD diffractometer (Bruker AXS, Madison, WI [27] using graphite-monochromatized Mo Kα radiation (λ = 0.71073 Å). For **PPA·HBA** and **PPAH·HBD** cocrystals, X-ray diffraction data were collected on a Bruker D8 VENTURE diffractometer with microfocus sealed tube using graphite-monochromatized Cu Kα radiation (λ = 1.54178 Å). SADABS program was used for absorption correction and scaling of observed data [28]. The structures were solved by direct methods and refined by full-matrix least-squares on F^2 for all data, using SHELXS97 [29] and OLEX 2.0 [30] software suites. The nonhydrogen atoms were refined in anisotropic approximation. The disorder was resolved for **PPA** in the pure form and in the 1:1 cocrystal **PPA·HBA**. The C–H atoms were fixed at idealized positions and refined with a riding-model approximation: C–H = 0.95–1.00 Å with Uiso(H) = 1.5 Ueq (C-methyl) and 1.2 Ueq (C) for other H atoms. The N–H and O–H hydrogens were located from the difference Fourier map or constrained. In cocrystal **PPAH·HBD** acetone solvent was disordered and the SQUEEZE procedure [31] was used to treat the diffused solvent in voids. The electron counts and the volume of associated voids indicated approximately one acetone solvent molecule per asymmetric unit. The sum formula reflected this ration. A check of the final CIF files (CCDC no.2247133-2247137) using PLATON did not show any missed symmetry. MERCURY2022.3.0 program (Cambridge Crystallographic Data Centre, Cambridge, UK)was used to make the molecular graphics [32].

2.4. Quantum Chemical Calculations

For the comparison of different enantiomers and their conformers quantum chemical calculations of total energy of **PPA** molecules in pure form (4 conformers), and in two cocrystals with **HBA, PPAH** in pure form and in cocrystal with **HBD** were carried out using GAUSSIAN 09 program package [33] and the B3LYP/6-311++G(d,p) level of theory [34]. The experimental X-ray coordinates were used for calculations. Correction on zero-point energy (ZPE) was included into molecular energy. A summary of results is presented in Table S1.

3. Results

Single crystal X-ray diffraction data, data collection, and structure refinement details are summarized in Table 1. Hydrogen bonding interactions were analyzed and finally calculated using the HTAB instruction in SHELXL [29], see Table 2.

Table 1. Crystal data for pure forms **PPA** and **PPAH** and cocrystals **PPA·HBA**, **PPA·2HBA**, and **PPAH·HBD**·(acetone solvate).

Compound	PPA	PPA·HBA	PPA·2HBA	PPAH	PPAH·HBD [a]
CCDC number	2247135	2247137	2247134	2247133	2247136
Empirical formula	$C_{12}H_{14}N_2O_2$	$C_{19}H_{20}N_2O_5$	$C_{26}H_{26}N_2O_8$	$C_{15}H_{19}N_3O_2$	$C_{25}H_{32}N_4O_5$
Formula weight	218.25	356.37	494.49	273.337	468.54
Temperature/K	150(2)	293(2)	150(2)	100(2)	173(2)
Crystal system	triclinic	monoclinic	triclinic	monoclinic	triclinic
Space group	*P*-1	$P2_1/c$	*P*-1	$P2_1/c$	*P*-1
a/Å	6.0917(17)	18.9326(3)	7.9851(8)	5.5613(8)	5.2285(3)
b/Å	10.782(3)	5.58410(10)	12.6900(12)	14.190(2)	13.2516(7)
c/Å	17.502(5)	18.7881(4)	13.6456(13)	18.170(3)	18.4515(9)
α/°	76.700(4)	90	107.579(3)	90	104.612(4)
β/°	85.742(5)	118.9220(10)	104.040(3)	91.034(5)	92.217(3)
γ/°	81.827(5)	90	107.749(3)	90	92.539(3)

Table 1. *Cont.*

Compound	PPA	PPA·HBA	PPA·2HBA	PPAH	PPAH·HBD [a]
Volume/$Å^3$	1106.3(5)	1738.57(6)	1167.0(2)	1433.7(4)	1234.22(12)
Z	4	4	2	4	2
ρ_{calc} g/cm^3	1.310	1.361	1.407	1.266	1.261
μ/mm^{-1}	0.091	0.825	0.105	0.086	0.726
F(000)	464	752	520	584	500
Crystal size/mm^3	0.6 × 0.2 × 0.2	0.34 × 0.34 × 0.06	0.3 × 0.2 × 0.2	0.3 × 0.15 × 0.05	0.21 × 0.1 × 0.08
Reflections collected	52871	39609	34754	2220	16835
Independent reflections	6646 [R_{int} = 0.0958]	2646 [R_{int} = 0.0595]	4124 [R_{int} = 0.0842]	2220	4272 [R_{int} = 0.0451]
Data/restraints/parameters	6646/254/406	2646/0/239	4124/190/452	2220/36/184	4272/0/277
Goodness-of-fit on F^2	1.028	1.059	1.044	1.034	0.857
Final R indexes R_1, wR_2 [$I \geq 2\sigma(I)$]	0.0484, 0.1090	0.0399, 0.1081	0.0438, 0.1033	0.0473, 0.1263	0.0519, 0.1426
Final R indexes [all data] R_1, wR_2	0.0957, 0.1300	0.0422, 0.1102	0.0787, 0.1189	0.0767, 0.1379	0.0582, 0.1523
Largest diff. peak/hole/e $Å^{-3}$	0.25/−0.25	0.32/−0.19	0.30/−0.20	0.356/−0.196	0.64/−0.28

[a] In the refinement, scattering from the disordered acetone molecule was taken into account with the “SQUEEZE” procedure.

Table 2. Hydrogen bonds in the studied cocrystals and in the **PPAH** pure form.

D-H···A	H···A/Å	d(D···A)/Å	∠D-H···A/°	Symmetry Transformation for Acceptor
		PPA·HBA		
O(5)-H(5)···O(1)	1.84	2.6638(18)	178.9	$x, 5/2 - y, z + 1/2$
N(2)-H(2A)···O(4)	2.10	2.936(2)	163.6	$x, y + 1, z$
N(2)-H(2B)···O(4)	2.23	2.9751(19)	144.9	$-x, 1 - y, 1 - z$
O(3)-H(3)···O(2)	1.83	2.6329(17)	166.0	$x, y - 1, z$
		PPA·2HBA		
N(2)-H(2A)···O(1)	1.97(3)	2.906(3)	174(2)	$2 - x, 1 - y, 1 - z$
N(2)-H(2B)···O(2)	2.12(3)	2.999(3)	169(2)	$1 - x, 1 - y, 1 - z$
O(3)-H(3B)···O(2)	1.78(3)	2.671(2)	176(2)	$3 - x, 2 - y, 1 - z$
O(5)-H(5B)···O(6)	1.710(17)	2.599(2)	175(2)	x, y, z
O(7)-H(7B)···O(4)	1.745(17)	2.636(2)	174(2)	$3 - x, 2 - y, 1 - z$
O(8)-H(8)···O(3)	1.95(3)	2.820(2)	174(2)	$1 - x, 1 - y, -z$
C(11)-H(11A)···O(6)	2.58	3.407(3)	142.6	$2 - x, 1 - y, 1 - z$
		PPAH		
N(2)-H(2)···O(2)	2.09	2.948(2)	163.3	$2 - x, 1 - y, 1 - z$
C(10)-H(10B)···O(2)	2.53	3.474(3)	159.7	$x - 1, y, z$
C(15)-H(15B)···O(1)	2.53	3.387(3)	146.1	$2 - x, 1/2 + y, 3/2 - z$

Table 2. *Cont.*

D-H⋯A	H⋯A/Å	d(D⋯A)/Å	∠D-H⋯A/°	Symmetry Transformation for Acceptor
		PPAH·HBD		
N(1)-H(1A)⋯O(2)	2.07	2.940(4)	172.5	$2-x, 1-y, 2-z$
N(1)-H(1B)⋯O(2)	2.26	3.064(4)	151.2	$x-1, y, z$
N(3)-H(3)⋯O(4)	2.07	2.924(4)	161.9	$1-x, 1-y, 1-z$
O(1)-H(6)⋯O(3)	1.83(5)	2.665(4)	170(5)	x, y, z
C(2)-H(2)⋯O(3)	2.53	3.217(5)	129.2	x, y, z
C(17)-H(17B)⋯O(4)	2.53	3.423(4)	150.2	$x-1, y, z$

3.1. Crystal Structures of *PPA* Pure Form, *PPA·HBA* and *PPA·2HBA* Cocrystals

Figure 1 reveals the contents of asymmetric units for **PPA**, **PPA·HBA**, and **PPA·2HBA** (the molecules with labelling schemes are summarized in Figure S1). To estimate if purchased **PPA** material represents a racemic mixture or enantiopure compound we carried out its diffraction study. It was found that this material was a racemate with two symmetrically independent molecular positions in the unit cell, each of which was occupied by either *R*- or *S*-enantiomers with almost equal ~50% occupation factor (Figure 1a). These results are very close to data previously published by Rekis et al. for *rac*-**PPA** [20]. The *rac*-**PPA** structure allowed the authors of the above mentioned paper to describe the molecular arrangement in this crystal as a solid solution of enantiomers. Such a situation is common for structures of enantiomers when *R*- and *S*-enantiomers are interchangeable due to their isosterism, or significant similarity of their molecular shapes [35–39]. It was also mentioned that conformational flexibility of enantiomers helps them to adjust to their positions in crystal lattice. For room-temperature crystal structure **PPA·HBA**, the disorder was not resolved during structure refinement (Figure 1b); however, thermal ellipsoids of the phenyl and pyrrolidone rings demonstrate hints of such disorder. For low-temperature structure **PPA·2HBA** the disorder model was found (Figure 1c) with occupancy factors of 0.510(6) and 0.490(6) for two disordered positions similar to the **PPA** pure form.

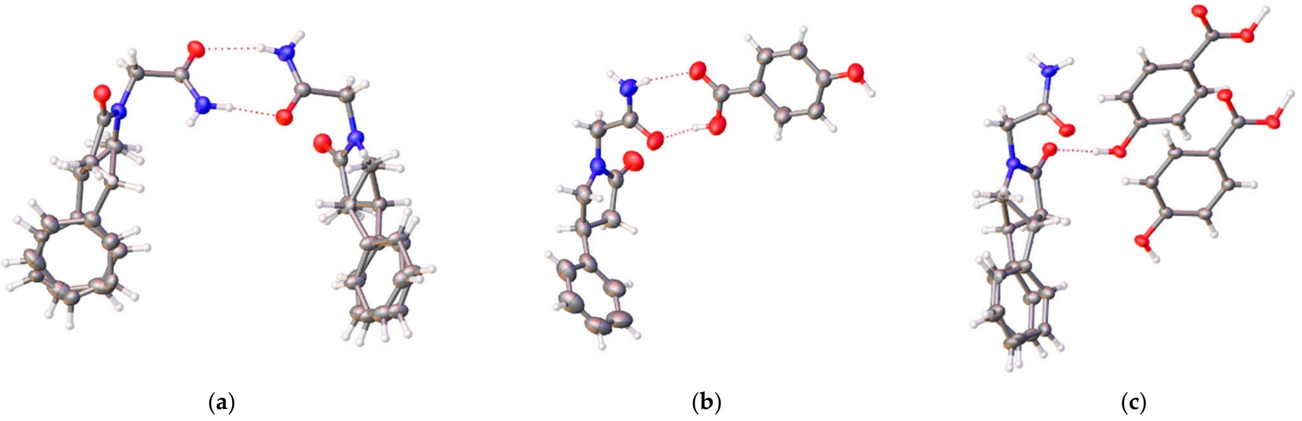
(**a**) (**b**) (**c**)

Figure 1. Contents of asymmetric units in: (**a**) **PPA** pure form, (**b**) **PPA·HBA,** and (**c**) **PPA·2HBA** cocrystals. Two disordered positions in **PPA** molecules are shown in Figure (**a**,**c**). Colorings scheme: oxygen—red; nitrogen—blue; carbon—grey; hydrogen—white, as used here and further.

Cocrystals **PPA·HBA** and **PPA·2HBA** were grown using the different ratios of starting materials (1:1 and 2:3, see Experimental Section). It is worth mentioning that variable stoichiometric ratios are not uncommon for API cocrystals [11,40,41].

The **PPA** molecule in **PPA**, **PPA·HBA**, and **PPA·2HBA** crystals demonstrates conformational flexibility. Figure 2 presents three examples of overlay of the molecular structures of the same enantiomers found in the above mentioned crystals. Absolute and relative molecular energies of the enantiomers with different conformations are given in Table S1. It is possible to see that energy differences between these structures are not large and related mostly to different orientations of amide and phenyl groups attached to the oxopyrrolidine ring.

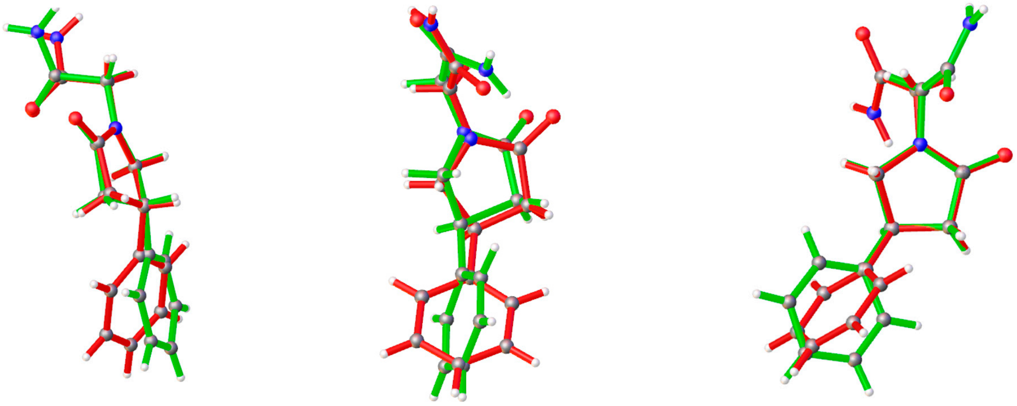

(**a**) (**b**) (**c**)

Figure 2. Selected examples of comparison of **PPA** molecular structure in crystals of **PPA·HBA**, and **PPA·2HBA**: (**a**) Overlay of *R*-enantiomers of **PPA** from **PPA·2HBA** (green) and from **PPA·HBA** (red); (**b**) Overlay of *S*-enantiomer of **PPA** from **PPA·2HBA** (green) and from **PPA·HBA** (red); (**c**) Overlay of *S*-enantiomer of **PPA** from **PPA·HBA** (green) and from **PPA·2HBA** (red).

In the 1:1 cocrystal, **PPA** and **HBA** molecules are interlinked via amide-carboxylic acid supramolecular heterosynthon (N···O= 2.936(2) Å, O···O = 2.6329(17) Å, Table 2) and dimerize in the centrosymmetric tetramer (N···O = 2.9751(19) Å) via fusion of three cyclic motifs in the sequence $R_2^2(8)R_4^2(8)R_2^2(8)$ (Figure 3a) [42]. Such tetrameric motif was previously registered in the **PA·HBA** cocrystal and in some other cocrystals with **HBA** coformer [11,43,44]. The H-bonded tetramers are further interlinked via the hydroxyl group of **HBA** and carbonyl of **PPA** molecules (O···O 2.6638(18) Å), thus affording the H-bonded layer situated parallel to the *bc* plane. All H-bonds are concentrated within this layer. The layers stack along the crystallographic *a*-axis with interdigitating **PPA** phenyl rings (Figure 3b).

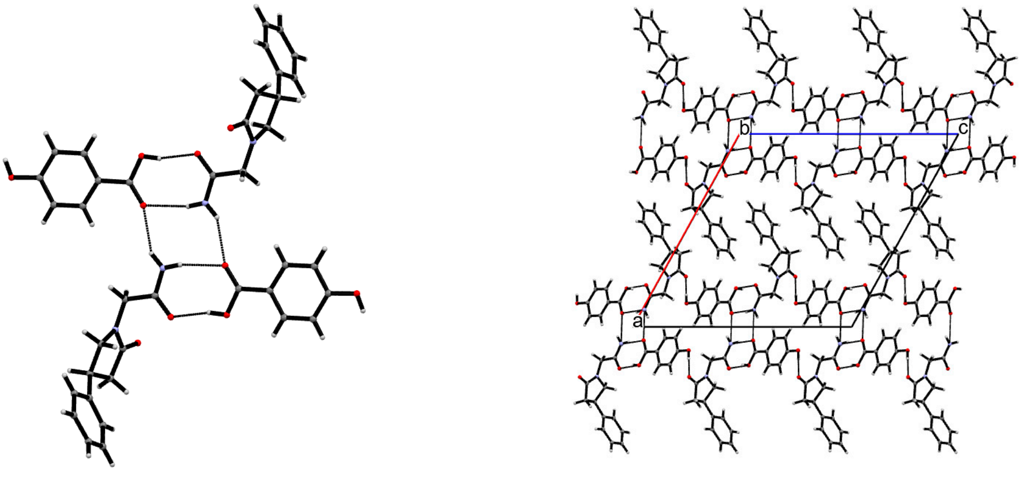

(**a**) (**b**)

Figure 3. 1:1 cocrystal **PPA·HBA**: (**a**) View of (**PPA**)$_2$(**HBA**)$_2$ H-bonded tetramer. (**b**) Packing of two H-bonded layers in the crystal, view along the *b*-axis.

In the 1:2 cocrystal, **PPA** and **HBA** molecules are self-assembled in two separate homomeric H-bonded motifs that are interconnected. The **PPA** H-bonded chain is formed via alternation of two centrosymmetric supramolecular homosynthons, namely the typical amide-amide $R_2^2(8)$ homosynthon (N···O = 2.906(3) Å) and the less common larger $R_2^2(14)$ homosynthon (N···O = 2.999(3) Å) (Figure 4a). The similar infinitive H-bonded motif was registered for **PA** in the **PA·HBA·H$_2$O** cocrystal [8] and for *rac*-**PPA** and *S*-**PPA** homomolecular forms (Figure 4b), except in the latter cases the amide-amide $R_2^2(8)$ homosynthons are non-centrosymmetric [20]. In the reported cocrystal, the **PPA** homomeric chains interdigitate forming the layer parallel to the (0 1-1) plane (Figure 4c) and stabilized by significantly less directional dispersion interactions (π(Ph)···π(Ph), CH(7)···π(Ph) = 2.1 Å) and weak C-H···O hydrogen bond (C···O = 3.42(2) Å). In turn, two chemically identical but crystallographically distinct **HBA** coformers are dimerized via robust $R_2^2(8)$ acid-acid supramolecular homosynthon (O···O = 2.671(2) Å and 2.599(2) Å) and form the tail-to-tail H-bonded chain via hydroxyl-groups (O···O = 2.636(2) Å) (Table 2). These carboxylic chains were also packed in the layers (Figure 4d). Similar to the 1:1 cocrystal, **HBA** and **PPA** interconnect through hydroxyl and carbonyl groups (O···O = 2.820(2) Å) that results in the 3D hydrogen bonded network where the homomeric **PPA** and **HBA** layers alternate (Figure S2). In addition to the already mentioned **PA**-hydroquinone cocrystal [8], **PA** and citric acid in cocrystal also form homomeric H-bonded domains that interconnect [10].

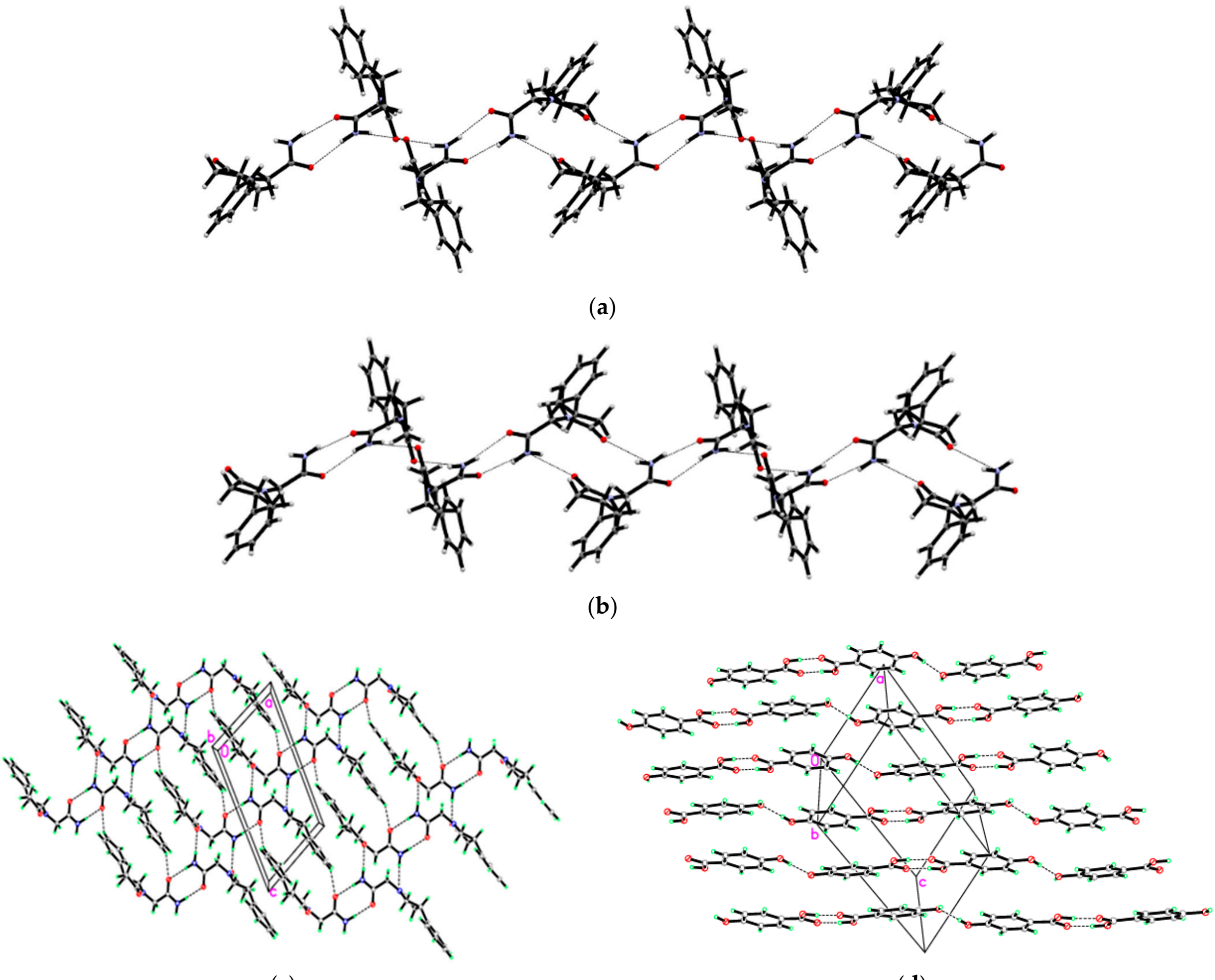

(**a**)

(**b**)

(**c**) (**d**)

Figure 4. Comparison of molecular synthons in *rac*-**PPA** and 1:2 cocrystal **PPA·2HBA**: (**a**) View of the **PPA** homomeric chain in **PPA·2HBA**; (**b**) **PPA** homomeric chain in *rac*-**PPA**; (**c**) Packing of **PPA** chains in the layer in cocrystal via CH···O short contacts and π-π stacking interactions between the phenyl rings. (**d**) Packing of **HBA** chains in stacking layer.

3.2. Crystal Structures of PPAH Pure Form and PPAH·HBD Cocrystal

Asymmetric units of **PPAH** and **PPAH·HBD** (the disordered acetone solvent molecule was excluded) crystals and overlapping diagram for **PPAH** from these two solids are shown in Figure 5a–c (for numbering see Figure S1). The geometrical parameters of the **PPAH** molecule are similar in the pure form and in the cocrystal. These similarities are evident from the overlay of these molecules presented in Figure 5c. Molecular energies of the **PPAH** molecule in pure crystal and in cocrystal are very close (Table S2).

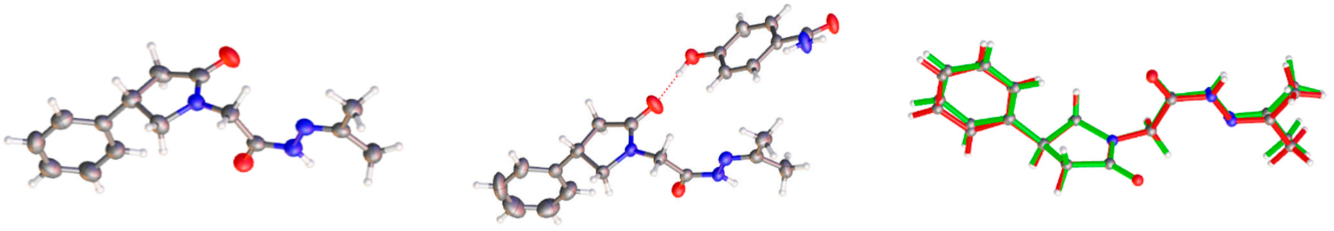

(**a**) (**b**) (**c**)

Figure 5. Content of asymmetric units in: (**a**) **PPAH**, (**b**) **PPAH·HBD** (see Supplementary Materials for structures with labels), and (**c**) overlay diagram for **PPAH** from pure material (green) and from cocrystal with **HBD** (red).

PPAH crystallizes in the monoclinic $P2_1/c$ space group with one molecule in the asymmetric unit. The expected dimerization of molecules occurs via amide-amide homosynthon, N···O = 2.948(2) Å (Figure 6a). The dimers pack in stacks along the shortest *a*-axis with only weak intermolecular CH···O interactions between stacks (Table 2, Figure 5b).

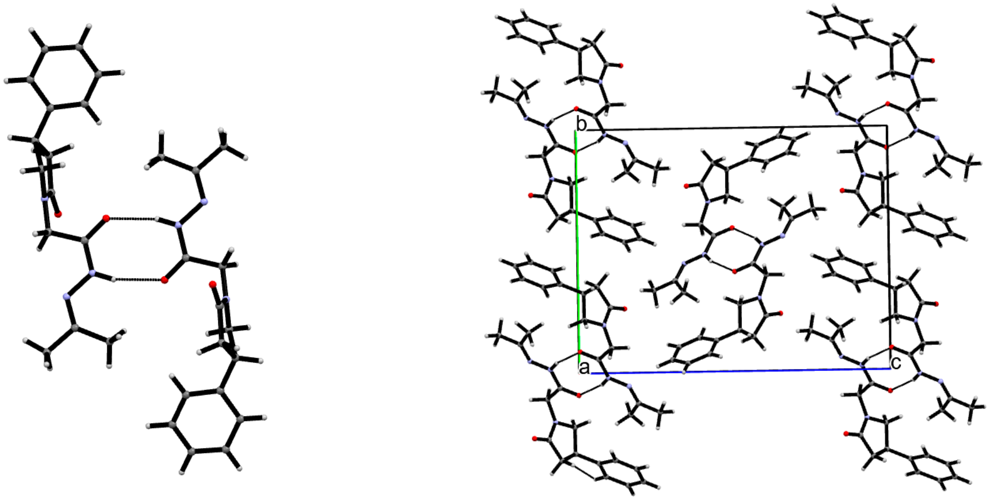

(**a**) (**b**)

Figure 6. (**a**) View of centrosymmetric dimer in **PPAH**, (**b**) packing of **PPAH** dimers in crystal, view along the *a*-axis.

In the **PPAH·HBD** cocrystal, the self-association of each component occurs via amide-amide homosynthon (Figure 7a,b). Similar to the pure form, the **PPAH** molecules in cocrystal form the centrosymmetric dimers (N···O = 2.924(4) Å), while **HBD** coformers form the H-bonded double chain where the amide-amide homosynthons are further interlinked via synthon's sequence … $R_2^2(8)R_4^2(8)R_2^2(8)$ … (N···O = 2.940(4), 3.064(4) Å, Table 2) identical with that found for $(\mathbf{PPA})_2(\mathbf{HBA})_2$ tetramers (Figure 2a). The discrete **PPAH** dimers and roughly planar **HBD** chains interconnect through **HBD** hydroxyl and **PPAH** carbonyl groups (O···O = 2.665(4) Å) resulting in the H-bonded layer (Figure 7c). An interesting feature is that the stacking pattern of **PPAH** in the pure form was conserved in cocrystal strengthening by the **PPAH**···**HBD** coformer H-bond (Figure S3). The packing of the layers remains voids of 241 Å^3 filled by the disordered acetone solvent (Figure S4).

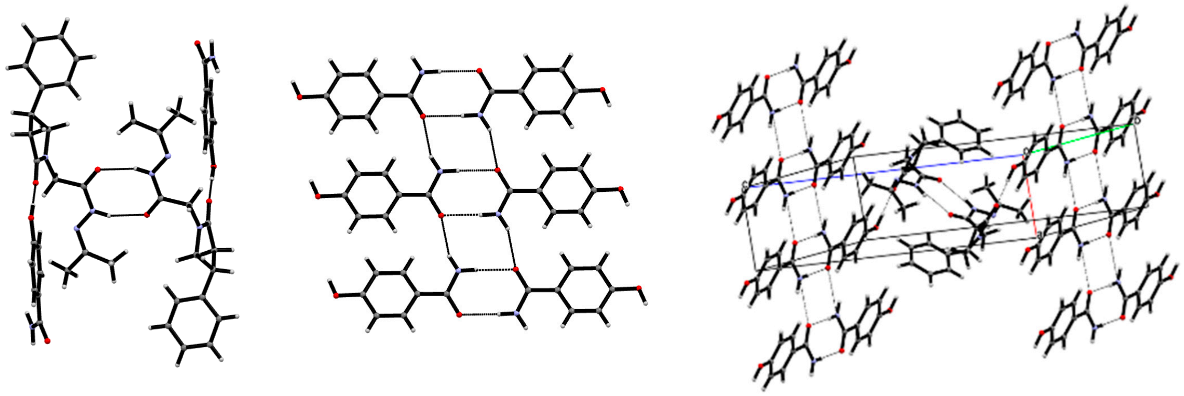
(**a**) (**b**) (**c**)

Figure 7. Cocrystal **PPAH·HBD**: (**a**) View of **PPAH** dimerization via amide-amide homosynthon with two **HBD** coformers attached to dimer via OH···O hydrogen bonds; (**b**) H-bonded double chain of **HBD** coformers; (**c**) Fragment of **PPAH·HBD** H-bonded layer, view along the *b*-axis.

Quantum chemical calculations of **PPA** and **PPAH** conformers found in the pure materials and cocrystals (see Supplementary Materials) demonstrated that energy differences for most conformers do not exceed 2 kcal/mol. Such a difference suggests that conformational variations of these molecules are mostly defined by influence of packing conditions (in this case R- and S-enantiomers intend to occupy same molecular position in crystal) on molecular conformation.

4. Conclusions

Two cocrystals of phenylpiracetam (**PPA**) with 4-hydroxybenzylcarboxylic acid (**HBA**) coformer with different stoichiometry and a cocrystal of 2-(4-phenyl-2-oxopyrrolidin-1-yl)-N′-isopropylideneacetohydrazide (**PPAH**) with 4-hydroxybenzamide (**HBD**) coformer were obtained by cocrystallization experiments. Despite the fact that both racetams contain a primary amide as a main functional group for hydrogen bonding, the structures of reported cocrystals are significantly different and dependent on the interplay of amide-amide, amide-carboxylic acid, carboxylic acid-carboxylic acid supramolecular homo- and heterosynthons. Otherwise, the hydroxyl–carbonyl heterosynthon was found in all three cocrystal structures with both coformers. The H-bonded homomeric chain found in the **PPA** *rac*- and enantiopure forms, was also present in the 1:2 cocrystal resulting in alternation of **PPA** and **HBA** homomeric regions. The dimerization of **PPAH** via amide-amide supramolecular homosynthon led to the identical stacking of this homodimer as a dominating motif both in the cocrystal and in the racetam pure form. **PPA** in two cocrystals, **PPA·HBA** and **PPA·2HBA** demonstrated conformational freedom originating from the lack of strong intermolecular interactions with participation of phenyl and oxopyrrolidine rings that was reflected in disorder registered for these moieties in the crystals. The described situation allowed us to consider these cocrystals as examples of partial solid solutions.

Supplementary Materials: The following supporting information can be downloaded at: https://www.mdpi.com/article/10.3390/chemistry5020074/s1, Figure S1. ORTEP drawings with labelling schemes; Figure S2. Alternation of homomeric **PPA** and **HBA** H-bonded layers in cocrystal **PPA·2HBA**; Figure S3. Similar packing motifs in **PPAH** and **PPAH·HBD** cocrystal; Figure S4. Packing of **PPAH·HBD** H-bonded layers with voids filled by the disordered acetone solvent molecules; Table S1. Relative energies of **PPA** enantiomers with different conformations according to DFT calculations on B3LYP/6-311++(d,p) level of theory, kcal/mol; Table S2. Relative energies of **PPAH** enantiomers with different conformations according to DFT calculations on B3LYP/6-311++(d,p) level of theory, kcal/mol.

Author Contributions: Conceptualization, J.M. and T.V.T.; methodology, M.S.F.; investigation, J.M., E.N., S.R., M.S.F., R.C., T.K. and T.V.T.; writing—original draft preparation, M.S.F. and T.V.T.; writing—review and editing, all authors; visualization, M.S.F., E.N. and S.R.; supervision, T.V.T.; project administration, T.V.T. and M.S.F.; funding acquisition, T.V.T. All authors have read and agreed to the published version of the manuscript.

Funding: This study was supported by **NSF DMR PREM** grants **#1523611** and **#2122108**. M.S.F. thanks the project **ANCD 20.80009.5007.15** for support.

Data Availability Statement: Any details are available from the authors. CCDC 2247133-2247137 contain the supplementary crystallographic data for this paper. These data can be obtained free of charge via www.ccdc.cam.ac.uk/data_request/cif, accessed on 8 March 2023, or by emailing data_request@ccdc.cam.ac.uk, or by contacting The Cambridge Crystallographic Data Centre, 12 Union Road, Cambridge CB2 1EZ, UK; fax: +44 1223 336033.

Acknowledgments: We thank Arkady Ellern for the help with data collection and structure solution of two presented crystalline materials.

Conflicts of Interest: The authors declare no conflict of interest.

References

1. Giurgea, C. The "Nootropic" Approach to the Pharmacology of the Integrative Activity of the Brain. *Cond. Refl.* **1973**, *8*, 108–115. [CrossRef]
2. Gustafson, L.; Risberg, J.; Johanson, M.; Fransson, M.; Maximilian, V.A. Effects of piracetam on regional cerebral blood flow and mental functions in patients with organic dementia. *PMC* **1978**, *56*, 115–117. [CrossRef]
3. Spignoli, G.; Pepeu, G. Interactions between oxiracetam, aniracetam and scopolamine on behavior and brain acetylcholine. *Pharmacol. Biochem. Behav.* **1987**, *27*, 491–495. [CrossRef] [PubMed]
4. Malykh, A.; Sadaie, M. Piracetam and Piracetam-Like Drugs from Basic Science to Novel Clinical Applications to CNS Disorders. *Drugs* **2010**, *70*, 287–312. [CrossRef] [PubMed]
5. *The Merck Index*, 13th ed.; Merck & Co. Inc.: Whitehouse Station, NJ, USA, 2001; p. 1342. Available online: http://www.ucbpharma.com/ (accessed on 1 March 2022).
6. Fabbiani, F.; Allan, D.; David, W.; Davidson, A.; Lennie, A.; Parsons, S.; Pulham, R.; Warren, J. High-Pressure Studies of Pharmaceuticals: An Exploration of the Behavior of Piracetam. *Cryst. Growth Des.* **2007**, *7*, 1115–1124. [CrossRef]
7. Leng, F.; Robeyns, K.; Leyssens, T.; Shemchuk, O. Combining Racetams with a Sweetener through Complexation. *Cryst. Growth Des.* **2022**, *22*, 3016–3023. [CrossRef]
8. Aitipamula, S.; Chow, P.; Tan, R. Structural, Spectroscopic and Thermal Analysis of Cocrystals of Carbamazepine and Piracetam with Hydroquinone. *J. Chem. Crystallogr.* **2011**, *41*, 1604–1611. [CrossRef]
9. Durán-Palma, M.; Mendoza-Barraza, S.; Magaña-Vergara, N.; Martínez-Martínez, F.; González-González, J. Crystal structure of pharmaceutical cocrystals of 2,6-diaminopyridine with piracetam and theophylline. *Acta Crystallogr. Sect. C Struct. Chem.* **2017**, *C73*, 767–772. [CrossRef]
10. Viertelhaus, M.; Hilfiker, R.; Blatter, F.; Neuburger, M. Piracetam Co-Crystals with OH-Group Functionalized Carboxylic Acids. *Cryst Growth Des.* **2009**, *9*, 2220–2228. [CrossRef]
11. Vishweshwar, P.; McMahon, J.; Peterson, M.; Hickey, M.; Shattock, T.; Zaworotko, M. Crystal engineering of pharmaceutical co-crystals from polymorphic active pharmaceutical ingredients. *Chem. Commun.* **2005**, 4601–4603. [CrossRef]
12. Abeysekera, A.M.; Averkiev, B.B.; Sinha, A.S.; Aakeröy, C.B. Evaluating structure–property relationship in a new family of mechanically flexible co-crystals. *Chem. Commun.* **2022**, *58*, 9480–9483. [CrossRef] [PubMed]
13. Aakeröy, C.B.; Alicia, M.; Beatty, A.M.; Brian, A.; Helfrich, B.A. A High-Yielding Supramolecular Reaction. *J. Am. Chem. Soc.* **2002**, *124*, 14425–14432. [CrossRef] [PubMed]
14. Saha, S.; Desiraju, G.R. Acid···Amide Supramolecular Synthon in Cocrystals: From Spectroscopic Detection to Property Engineering. *J. Am. Chem. Soc.* **2018**, *140*, 6361–6373. [CrossRef]
15. Bolla, G.; Sarma, B.; Nangia, A.K. Crystal Engineering of Pharmaceutical Cocrystals in the Discovery and Development of Improved Drugs. *Chem. Rev.* **2022**, *122*, 11514–11603. [CrossRef]
16. Sowa, M.; Slepokura, K.; Matczak-Jon, E. A 1:1 pharmaceutical cocrystal of myricetin in combination with uncommon piracetam conformer: X-ray single crystal analysis and mechanochemical synthesis. *J. Mol. Str.* **2014**, *1058*, 114–121. [CrossRef]
17. Springuel, G.; Norberg, B.; Robeyns, K.; Wouters, J.; Leyssens, T. Advances in Pharmaceutical Co-crystal Screening: Effective Cocrystal Screening through Structural Resemblance. *Cryst. Growth Des.* **2012**, *12*, 475–484. [CrossRef]
18. Thomas, L.; Wales, C.; Wilson, C. Selective preparation of elusive and alternative single component polymorphic solid forms through multi-component crystallisation routes. *Chem. Commun.* **2016**, *52*, 7372–7375. [CrossRef]
19. Gorodnicheva, N.V.; Vasil´eva, O.S.; Ostroglyadov, E.S.; Baichurin, R.I.; Makarenko, S.V.; Karamov, F.A.; Lodochnikova, O.A.; Litvinov, I.A. 2-[4-(Het)aryl-2-oxopyrrolidin-1-yl]acetohydrazides: Synthesis, structures, and reactions with carbonyl compounds. *Russ. Chem. Bull. Int. Ed.* **2020**, *69*, 996–1008. [CrossRef]

20. Rekis, T.; Bērziņš, A.; Orola, L.; Holczbauer, T.; Actiņš, A.; Seidel-Morgenstern, A.; Lorenz, H. Single Enantiomer's Urge to Crystallize in Centrosymmetric Space Groups: Solid Solutions of Phenylpiracetam. *Cryst. Growth Des.* **2017**, *17*, 1411–1418. [CrossRef]
21. Groom, C.R.; Bruno, I.J.; Lightfoot, M.P.; Ward, S.C. The Cambridge Structural Database. *Acta Crystallogr. Sect. B Struct. Sci. Cryst. Eng. Mater.* **2016**, *B72*, 171–179. [CrossRef]
22. Zvejniece, L.; Svalbe, B.; Veinberg, G.; Grinberga, S.; Vorona, M.; Kalvinsh, I.; Dambrova, M. Investigation into Stereoselective Pharmacological Activity of Phenotropil. *Basic Clin. Pharmacol. Toxicol.* **2011**, *109*, 407–412. [CrossRef] [PubMed]
23. Childs, S.L.; Hardcastle, K.I. Cocrystals of Piroxicam with Carboxylic Acids. *Cryst. Growth Des.* **2007**, *7*, 1291–1304. [CrossRef]
24. Sanphui, P.; Mishra, M.K.; Ramamurty, U.; Desiraju, G.R. Tuning Mechanical Properties of Pharmaceutical Crystals with Multicomponent Crystals: Voriconazole as a Case Study. *Mol. Pharm.* **2015**, *12*, 889–897. [CrossRef] [PubMed]
25. Costa, R.N.; Reviglio, A.L.; Siedler, S.; Cardoso, S.G.; Linck, Y.G.; Monti, G.A.; Carvalho, A.M.G.; Resende, J.A.L.C.; Chaves, M.H.C.; Rocha, H.V.A.; et al. New Multicomponent Forms of the Antiretroviral Nevirapine with Improved Dissolution Performance. *Cryst. Growth Des.* **2020**, *20*, 688–698. [CrossRef]
26. Gohel, S.K.; Palanisamy, V.; Sanphui, P.; Prakash, M.; Singh, G.P.; Chernyshev, V. Isostructural cocrystals of metaxalone with improved dissolution characteristics. *RSC Adv.* **2021**, *11*, 30689–30700. [CrossRef]
27. Bruker. *APEX 2 Software for Crystal Structure Data Collection, Refinement and Structure Solution*; Bruker AXS Inc.: Madison, WI, USA, 2006.
28. *SADABS*, version 2.10; Bruker Analytical X-ray Systems, Inc.: Madison, WI, USA, 2003.
29. Sheldrick, G.M. A short history of SHELX. *Acta Crystallogr. Sect. A Found. Adv.* **2008**, *A64*, 112–122. [CrossRef]
30. Dolomanov, O.V.; Bourhis, L.J.; Gildea, R.J.; Howard, J.A.K.; Puschmann, H. *OLEX2*: A complete structure solution, refinement and analysis program. *J. Appl. Crystallogr.* **2009**, *42*, 339–341. [CrossRef]
31. Spek, A.L. *PLATON* SQUEEZE: A tool for the calculation of the disordered solvent contribution to the calculated structure factors. *Acta Crystallogr. Sect. C Struct. Chem.* **2015**, *C71*, 9–18. [CrossRef]
32. Macrae, C.F.; Bruno, I.J.; Chisholm, J.A.; Edgington, P.R.; McCabe, P.; Pidcock, E.; Rodriguez-Monge, L.; Taylor, R.; van de Streek, J.; Wood, P.A. *Mercury CSD 2.0*—new features for the visualization and investigation of crystal structures. *J. Appl. Crystallogr.* **2008**, *41*, 466–470. [CrossRef]
33. Frisch, M.J.; Trucks, G.W.; Schlegel, H.B.; Scuseria, G.E.; Robb, M.A.; Cheeseman, J.R.; Scalmani, G.; Barone, V.; Mennucci, B.; Petersson, G.A.; et al. *Gaussian 09, Revision C.01*; Gaussian, Inc.: Wallingford, CT, USA, 2009.
34. Alvarez, M.; Saavedra, E.; Olivella, M.; Suvire, F.; Zamora, M.; Enriz, R. Theoretical study of the conformational energy hypersurface of cyclotrisarcosyl. *Open Chem.* **2012**, *10*, 248–255. [CrossRef]
35. Kitaigorodsky, A.I. *Mixed Crystals*; Springer Series in Solid-state Sciences; Springer: Berlin/Heidelberg, Germany, 1984; ISBN 13: 978-3-642-81674-1.
36. Jacques, J.; Collet, A.; Wilen, S.H. *Enantiomers, Racemates, and Resolutions*; Krieger Publishing: Malabar, FL, USA, 1991.
37. Brandel, C.; Petit, S.; Cartigny, Y.; Coquerel, G. Structural aspects of solid solutions of enantiomers. *Curr. Pharm. Des.* **2016**, *22*, 4929–4941. [CrossRef] [PubMed]
38. Lodochnikova, O.A.; Kosolapova, L.S.; Saifina, A.F.; Gubaidullin, A.T.; Fayzullin, R.R.; Khamatgalimov, A.R.; Litvinov, I.A.; Kurbangalieva, A.R. Structural aspects of partial solid solution formation: Two crystalline modifications of a chiral derivative of 1,5-dihydro-2H-pyrrol-2-one under consideration. *CrystEngComm* **2017**, *19*, 7277–7286. [CrossRef]
39. Castañeda, R.; Lindeman, S.V.; Krivoshein, A.V.; Metta-Magaña, A.J.; Chen, Y.; Timofeeva, T.V. Remarkable Similarity of Molecular Packing in Crystals of Racemic and Enantiopure 2-Phenylpropionamide: $Z' = 4$ Structures, Molecular Disorder, and the Formation of a Partial Solid Solution. *Cryst. Growth Des.* **2022**, *22*, 4592–4600. [CrossRef]
40. Samipillai, M.; Rohani, S. The role of higher coformer stoichiometry ratio in pharmaceutical cocrystals for improving their solid-state properties: The cocrystals of progesterone and 4-hydroxybenzoic acid. *J. Cryst. Growth* **2019**, *507*, 270–282. [CrossRef]
41. Saikia, B.; Pathaka, D.; Sarma, B. Variable stoichiometry cocrystals: Occurrence and significance. *CrystEngComm* **2021**, *23*, 4583–4606. [CrossRef]
42. Bernstein, J.; Davis, R.E.; Shimoni, L.; Chang, N.-L. Patterns in Hydrogen Bonding: Functionality and Graph Set Analysis in Crystals. *Angew. Chem. Int. Ed.* **1995**, *34*, 1555–1573. [CrossRef]
43. Palanisamy, V.; Sanphui, P.; Bolla, G.; Narayan, A.; Seaton, C.C.; Vangala, V.R. Intriguing High Z″ Cocrystals of Emtricitabine. *Cryst. Growth Des.* **2020**, *20*, 4886–4891. [CrossRef]
44. Arenas-García, J.I.; Herrera-Ruiz, D.; Mondragón-Vásquez, K.; Morales-Rojas, H.; Höpfl, H. Co-Crystals of Active Pharmaceutical Ingredients—Acetazolamide. *Cryst. Growth Des.* **2010**, *10*, 3732–3742. [CrossRef]